Laser-Based Approach to Verify Nuclear Excitation by Electron Capture: Supplemental Material

Jintao Qi,[1,*] Boqun Liu,[1,*] and Xu Wang[1,2,†]

[1] *Graduate School, China Academy of Engineering Physics, Beijing 100193, China*

[2] *Southern Center for Nuclear-Science Theory, Institute of Modern Physics, Chinese Academy of Sciences, Huizhou, Guangdong 516000, China*

(Dated: September 1, 2024)

1. Theoretical framework of NEEC, NEIES, and NEET

The system's overall state is described as the product of the nuclear state $|IM\rangle$ with quantum numbers I and M, the electron state $|\psi\rangle$, and the photon number state $|n\rangle$. The initial and final states are denoted as i and f:

$$\begin{aligned} |i\rangle &= |I_i M_i\rangle \otimes |\psi_i\rangle \otimes |0\rangle\,, \\ |f\rangle &= |I_f M_f\rangle \otimes |\psi_f\rangle \otimes |0\rangle\,. \end{aligned} \tag{S1}$$

The interaction Hamiltonian H_I is given by [S1]

$$H_I = -\frac{1}{c}\int [\mathbf{J}_n(\mathbf{r}) + \mathbf{J}_e(\mathbf{r})]\cdot \mathbf{A}(\mathbf{r})\mathrm{d}\tau + \int \frac{\rho_n(\mathbf{r})\rho_e(\mathbf{r}')}{|\mathbf{r}-\mathbf{r}'|}\mathrm{d}\tau\mathrm{d}\tau'. \tag{S2}$$

Here, $\rho_{n/e}$ and $\mathbf{J}_{n/e}$ denote the charge density and current density of the nucleus or electron, respectively. $\mathbf{A}(\mathbf{r})$ is the vector potential of the radiation field. With the aid of multipole expansions, the interaction matrix element can be expressed as

$$\begin{aligned} \langle f|\, H_I\, |i\rangle = \sum_{\lambda\mu} \frac{4\pi}{2\lambda+1}(-1)^{\mu}\big[&\langle\psi_f|\, \hat{\mathcal{N}}^{E}_{\lambda\mu}\, |\psi_i\rangle \langle I_f M_f|\, \hat{\mathcal{M}}^{E}_{\lambda,-\mu}\, |I_i M_i\rangle \\ &- \langle\psi_f|\, \hat{\mathcal{N}}^{M}_{\lambda\mu}\, |\psi_i\rangle \langle I_f M_f|\, \hat{\mathcal{M}}^{M}_{\lambda,-\mu}\, |I_i M_i\rangle\big]. \end{aligned} \tag{S3}$$

In this context, $\hat{\mathcal{N}}^{E/M}_{\lambda\mu}$ and $\hat{\mathcal{M}}^{E/M}_{\lambda\mu}$ represent electric (labeled by E) or magnetic (labeled by M) multipole transition operators of the electron and the nucleus, respectively, characterized by the angular quantum number λ and the magnetic quantum number μ [S1]. The reduced nuclear transition probability $B(E/M; I_i \to I_f)$ is introduced:

$$B(E/M; I_i \to I_f) = \frac{1}{2I_i+1}\sum_{M_i M_f \mu} |\, \langle I_f M_f|\, \hat{\mathcal{M}}^{M}_{\lambda,\mu}\, |I_i M_i\rangle\, |^2. \tag{S4}$$

In this study, the transition from the nuclear ground state to the isomeric state of ^{235}U is predominantly of type $E3$, and a value of $B(E3) = 0.009$ W.u. is employed, as given in [S2, S3].

1.1 Cross sections of NEEC and NEIES

In NEEC (NEIES), the nucleus undergoes excitation as a result of the energy released from electron free-bound (free-free) transitions. In this study, we utilize Dirac distorted waves (DWs) to characterize the electron free states, as outlined in Ref. [S4]:

$$\psi_{\mathbf{p}\nu}^{(\pm)} = 4\pi\sqrt{\frac{\varepsilon+c^2}{2E}}\sum_{jlm}[\Omega_{\kappa m}^{*}(\mathbf{v})\chi_\nu]\mathrm{e}^{\pm\mathrm{i}\delta_{jl}}\begin{pmatrix} g_{jl}(r)\Omega_{\kappa m}(\hat{r}) \\ \\ -if_{jl'}(r)\Omega_{-\kappa m}(\hat{r}) \end{pmatrix}, \tag{S5}$$

where δ_{jl} is the total phase shift of the corresponding partial wave, and the connection between momentum p and energy ε is given by $\varepsilon = c\sqrt{p^2+c^2}$. The electron in the initial (final) state is associated with the + (−) sign for the phase shift. The electron bound states are determined by the solutions of the Dirac equation [S4]:

$$\psi_{n\kappa m} = \begin{pmatrix} g_{n\kappa}(r)\Omega_{\kappa m}(\hat{r}) \\ \\ -if_{n\kappa}(r)\Omega_{-\kappa m}(\hat{r}) \end{pmatrix}, \tag{S6}$$

where n is the principal quantum number, m is the magnetic quantum number, and κ serves as a shorthand notation for the total angular quantum number j and the orbital angular quantum number l as $\kappa = (l-j)(2j+1)$. Furthermore, $g_{n\kappa}(r)$ and $f_{n\kappa}(r)$ denote the radial wave functions for the upper and lower components, respectively. The spherical spinors $\Omega_{\kappa m}$ are defined as:

$$\Omega_{\kappa m}(\hat{r}) = \sum_{\nu=\pm 1/2}\langle l, 1/2, m-\nu, \nu | j, m\rangle\, Y_{l,m-\nu}(\hat{r})\chi_\nu, \tag{S7}$$

where the spinor χ_ν has the two components:

$$\chi_{1/2} = (1,\ 0)^T, \quad \chi_{-1/2} = (0,\ 1)^T. \tag{S8}$$

The cross section for NEEC is expressed as

$$\begin{aligned}\sigma_{\mathrm{NEEC}}(\varepsilon_i) =& \frac{1}{v_i}|\left\langle f\right| H_I \left|i\right\rangle|^2 \frac{\Gamma_f}{\delta_{if}^2+\Gamma_f^2/4} \\ =& \frac{4\pi^2}{c^2}\frac{\varepsilon_i+c^2}{p_i^3}\frac{k_{\mathrm{is}}^{2\lambda+2}}{[(2\lambda+1)!!]^2}B(E\lambda; I_i\to I_f)\frac{\Gamma_f}{\delta_{if}^2+\Gamma_f^2/4} \\ & \times\sum_{l_i,j_i}(2j_i+1)(C_{j_i 1/2\lambda 0}^{j_f 1/2})^2|\mathcal{R}_{E\lambda}^{if}|^2.\end{aligned} \tag{S9}$$

In this equation, δ_{if} is the energy mismatch between the nuclear and atomic transitions, given by $\delta_{if} = (\varepsilon_i - \varepsilon_f) - \varepsilon_{\mathrm{is}}$, where ε_i and ε_f denote the initial and final energy of the electron. The

wavenumber corresponding to the nuclear isomeric transition is denoted as $k_{\rm is} = E_{\rm is}/c$. Γ_f is the linewidth of the final atomic state. $C^{j_f 1/2}_{j_i 1/2 \lambda 0}$ is a Clebsch-Gordan coefficient:

$$(C^{j_f 1/2}_{j_i 1/2 \lambda 0})^2 = (2l_i+1)(2l_f+1)(2j_f+1) \begin{pmatrix} l_f & l_i & \lambda \\ 0 & 0 & 0 \end{pmatrix}^2 \begin{Bmatrix} l_i & \lambda & l_f \\ j_f & \frac{1}{2} & j_i \end{Bmatrix}^2 . \tag{S10}$$

In the expressions involving the parentheses and curly brackets, the six-component entities correspond to the Wigner 3-j and 6-j symbols, respectively. The radial matrix element $\mathcal{R}^{if}_{E\lambda}$ is given by the integral:

$$\mathcal{R}^{if}_{E\lambda} = \int_0^\infty \left[g_i(r) g_f(r) + f_i(r) f_f(r) \right] h_\lambda(k_{\rm is} r) r^2 {\rm d}r, \tag{S11}$$

where h_λ is the spherical Hankel function.

When the energy of the incoming electron follows a specific distribution, integrating over the free electron's energy becomes necessary. The resonant strength, denoted as $S_{\rm NEEC}$, turns out to be a sensible quality:

$$S_{\rm NEEC} = \int d\varepsilon_i \sigma_{\rm NEEC}(\varepsilon_i). \tag{S12}$$

In Fig. S1, we present the 20 most efficient NEEC channels for ^{235}U ions with charges ranging from 1^+ to 10^+. In our calculations the maximum angular quantum number is set to be $l = 50$, including over 500 potential excited states.

The cross section for NEIES is given by [S5, S6]

$$\begin{aligned} \sigma_{\rm NEIES}(\varepsilon_i) =& \frac{8\pi^2}{c^4} \frac{\varepsilon_i + c^2}{p_i^3} \frac{\varepsilon_f + c^2}{p_f} B(E\lambda; I_i \to I_f) \frac{k_{\rm is}^{2\lambda+2}}{[(2\lambda+1)!!]^2} \\ & \times \sum_{l_i, j_i, l_f, j_f} (2j_i+1)(C^{j_f 1/2}_{j_i 1/2 \lambda 0})^2 |\mathcal{R}^{if}_{E\lambda}|^2, \end{aligned} \tag{S13}$$

where ε_i and ε_f denote the initial and final energies of the free electron, respectively, and $\varepsilon_i = \varepsilon_f + \varepsilon_{\rm is}$.

1.2 Excitation rate of NEET

In NEET, the nucleus experiences excitation through electron bound-bound transitions, with the electron bound states described by Eq. (S6). The NEET transition rate from atomic state i

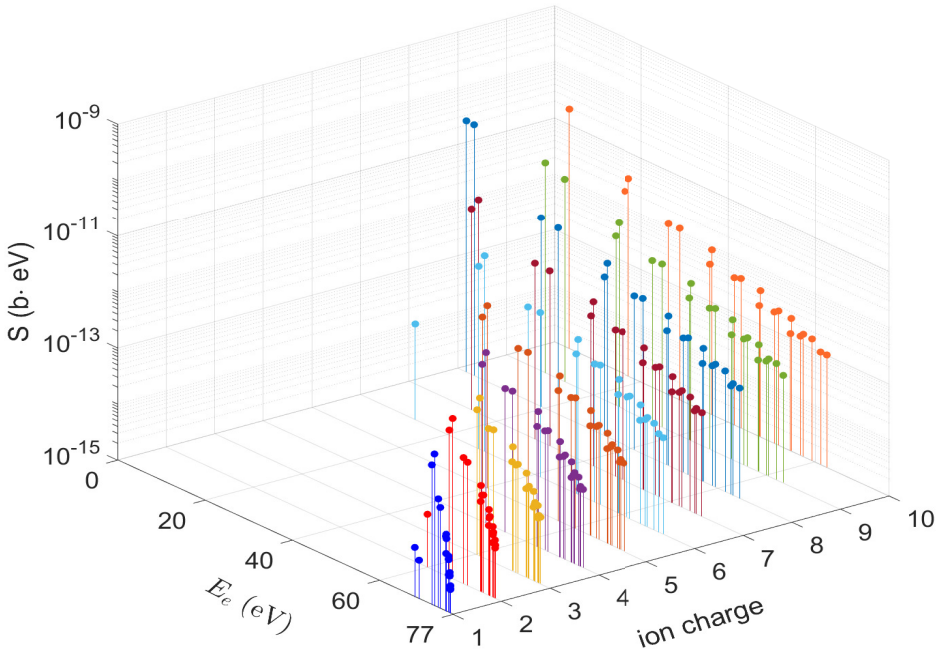

FIG. S1: The resonant strength of NEEC for charge states from 1^+ to 10^+. The top 20 NEEC channels are shown for each ionic state. The excitation energy of ^{235m}U is 76.7 eV.

to state f of a U^{q+} ion is expressed as [S7]:

$$\begin{aligned} W_{\mathrm{NEET}}^{q,i} &= \left(1+\frac{\Gamma_i}{\Gamma_f}\right)\frac{|\langle f|H_I|i\rangle|^2}{\delta_{if}^2+(\Gamma_f+\Gamma_i)^2/4} \\ &= \frac{4\pi k_{\mathrm{is}}^{2\lambda+2}}{[(2\lambda+1)!!]^2}B(E\lambda;I_i\to I_f)(C_{j_i 1/2\lambda 0}^{j_f 1/2})^2|\mathcal{R}_{E\lambda}^{if}|^2\left(1+\frac{\Gamma_i}{\Gamma_f}\right)\frac{1}{\delta_{if}^2+(\Gamma_f+\Gamma_i)^2/4}. \end{aligned} \tag{S14}$$

Here, Γ_i and Γ_f denote the linewidths of the initial and final atomic states, respectively.

1.3 Broadening effects on NEET

Following laser-cluster interaction, a nanometer plasma is generated, introducing thermal motions in electrons and ions that result in broadening effects on electron bound states. Consequently, both Stark broadening and Doppler broadening effects are taken into account in this study. From Ref. [S8], the Stark width can be expressed as:

$$\Gamma_S = 9.16\times10^{-19}(1-0.7N_D^{-1/3})(2\pi c)(n_i^2-n_f^2)Z_p^{1/3}n_e^{2/3}. \tag{S15}$$

Here, N_D represents the number of particles in the Debye sphere, given by $N_D = 1.72\times10^9\sqrt{T_e^3/n_e}$. The parameters n_e and T_e denote the electron density in cm^{-3} and the temperature in eV, respec-

tively. n_i (n_f) corresponds to the principal quantum number of the initial (final) state, and Z_p represents the charge of the ion. The Doppler width is determined by the formula [S9]

$$\Gamma_D = \omega_0 \sqrt{8 \ln^2 \left(\frac{kT}{Mc^2} \right)}, \tag{S16}$$

where ω_0 represents the central angular frequency and M is the mass of the ^{235}U ion.

The linewidth of the atomic state can be written as $\Gamma = \Gamma_R + \Gamma_S + \Gamma_D$, where the natural width Γ_R for an electron bound state is typically on the order of 10^{-5} eV. In the nanometer-plasma, the electron density is approximately $10^{22} - 10^{23}$ cm^{-3} and the temperature ranges from $1 - 10$ eV. The estimated Stark width is $0.1 - 1$ eV, while the Doppler width is on the order of 10^{-3} eV. The Stark width is the dominant contributor to the linewidth of atomic states.

In clusters characterized by high electron density, enhanced broadening facilitates both NEET and NEEC processes. The energy levels and wave functions of ionic states are computed utilizing the RADIAL code [S10], employing a Dirac-Hartree-Fock-Slater method. The most efficient NEET channels for U^{7+} and U^{8+} ions are detailed in TABLE S1 and S2. The calculation results of isomer production yields via NEET in laser-heated clusters will be presented in the following section.

TABLE S1: Major NEET channels in U^{7+}

Transition channel	ΔE (eV)	V_{if}^2 (eV^2)	Rate (s^{-1})
$6g_{\frac{7}{2}} \rightarrow 6p_{\frac{3}{2}}$	1.1×10^{-2}	1.09×10^{-30}	1.01×10^{-16}
$6g_{\frac{9}{2}} \rightarrow 6p_{\frac{3}{2}}$	1.07×10^{-2}	2.87×10^{-29}	2.79×10^{-15}
$9f_{\frac{5}{2}} \rightarrow 5d_{\frac{3}{2}}$	1.34×10^{-2}	6.58×10^{-23}	4.51×10^{-10}
$9f_{\frac{5}{2}} \rightarrow 5d_{\frac{5}{2}}$	6.01×10^{-3}	2.45×10^{-23}	1.47×10^{-9}

TABLE S2: Major NEET channels in U^{8+}

Transition channel	ΔE (eV)	V_{if}^2 (eV^2)	Rate (s^{-1})
$8f_{\frac{7}{2}} \rightarrow 5d_{\frac{5}{2}}$	4.36×10^{-4}	1.59×10^{-23}	1.90×10^{-8}
$13d_{\frac{3}{2}} \rightarrow 6p_{\frac{3}{2}}$	6.92×10^{-3}	1.46×10^{-21}	2.36×10^{-8}
$14d_{\frac{5}{2}} \rightarrow 6p_{\frac{1}{2}}$	5.84×10^{-3}	2.92×10^{-21}	4.79×10^{-10}
$14d_{\frac{5}{2}} \rightarrow 6p_{\frac{3}{2}}$	2.21×10^{-3}	6.49×10^{-22}	1.11×10^{-10}

2. NEET yield in laser-heated ^{235}U clusters

In the cluster plasma, the probability of an ionic state i is given by the Boltzmann distribution:

$$p_i = \frac{1}{G} \exp\left(-\frac{\varepsilon_i}{T_e}\right), \tag{S17}$$

where ε_i is the energy of state i above the ground state in eV, T_e is the temperature in eV, and $G = \sum_j \exp(-\varepsilon_j/T_e)$ is the normalization denominator for all accessible states (i.e. the partition function). The isomer production yield per cluster via NEET can be written as

$$Y_{\mathrm{NEET}} = N_{ion} \int_0^t dt' \sum_q P_q(t') \sum_i p_{q,i}(t') W^{q,i}_{\mathrm{NEET}}, \tag{S18}$$

where N_{ion} is the number of ^{235}U ions per cluster (assumed to be 10^6 in this study). P_q is the probability to find a $^{235}U^{q+}$ ion in the cluster, and $p_{q,i}$ is the probability for the $^{235}U^{q+}$ ion in the i state. $W^{q,i}_{\mathrm{NEET}}$ is the NEET rate for the $^{235}U^{q+}$ ion of i state calculated using Eq. (S14).

Fig. S2 shows the isomer production yield per cluster via NEEC, NEIES, and NEET after the laser-cluster interaction for different wavelengths of 800 nm, 1600 nm, 2000 nm, and 2400 nm. The laser pulse duration is 30 femtoseconds (fs) FWHM. One sees that for all the cases, NEET is at least several orders of magnitude lower than NEIES or NEEC.

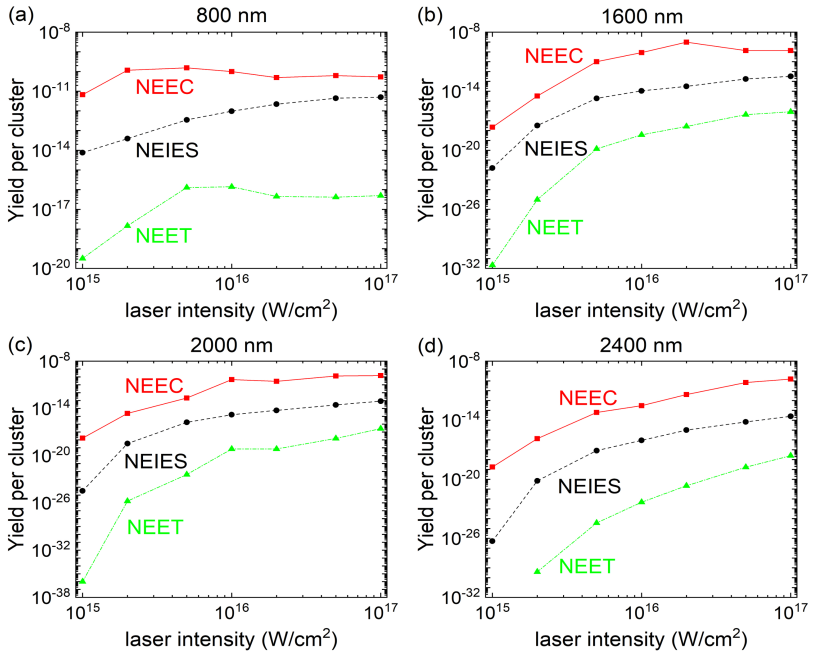

FIG. S2: Isomer production yield per cluster through NEEC, NEIES, and NEET at time 5 ps. The laser intensity varies from 10^{15} to 10^{17} W/cm^2, while the pulse duration is maintained at 30 fs. The laser wavelengths are as labeled on each figure: (a) 800 nm, (b) 1600 nm, (c) 2000 nm, and (d) 2400 nm.

3. Photoexcitation processes

In addition to electron-nucleus interactions, photoexcitation processes also come into play in laser-heated clusters, including: (1) Direct excitation by the fs laser pulse; (2) Photoexcitation by blackbody radiations; (3) Photoexcitation by bremsstrahlung. This section explores the effects of photoexcitation and concludes that the photoexcitation is insignificant in the isomer generation.

3.1 Direct laser excitation

The probability P_{if} of direct laser excitation can be expressed in terms of the amplitudes b_{if} for a transition from the nuclear ground state $|I_i M_i\rangle$ to the isomeric state $|I_f M_f\rangle$, as given by

$$P_{if}(t) = \frac{1}{2I_i+1} \sum_{M_i M_f} |b_{if}(t)|^2. \tag{S19}$$

The propability amplitude can be expressed as

$$b_{if}(t) = -\frac{i}{\hbar} \int_0^t \langle I_f M_f | H_l(t') | I_i M_i \rangle e^{i\omega_0 t'} dt' \ , \tag{S20}$$

where $\omega_0 = \varepsilon_{\rm is}/\hbar$ is the transition frequency of the isomeric state. The interaction Hamiltonian $H_l(t) = c^{-1} \int d\tau \boldsymbol{j}_n(\boldsymbol{r}) \cdot \boldsymbol{A}(\boldsymbol{r}, t)$, where $\boldsymbol{j}_n$ is the nuclear charge current and $\boldsymbol{A}(\boldsymbol{r}, t)$ is the vector potential of the laser field. The interaction matrix $\langle I_f M_f | H_l(t) | I_i M_i \rangle$ can be expressed using multipole expansions, consisting of electric and magnetic components [S11].

For the magnetic transitions, the matrix element is given by:

$$\langle I_f M_f | H_l(t) | I_i M_i \rangle = A(t)\sqrt{2\pi}\sqrt{\frac{\lambda+1}{\lambda}} \frac{k^\lambda}{(2\lambda+1)!!} C^{I_f M_f}_{I_i - M_i \lambda 0} \sqrt{2I_i+1} \sqrt{B(M\lambda; I_i \to I_f)} \ . \tag{S21}$$

Similarly for the electric transitions, the matrix element is:

$$\langle I_f M_f | H_l(t) | I_i M_i \rangle = A(t)\sqrt{2\pi}\sqrt{\frac{(2\lambda+1)(\lambda+1)}{\lambda}} \frac{k^\lambda}{(2\lambda+1)!!} C^{I_f M_f}_{I_i - M_i \lambda 0} \sqrt{2I_i+1} \sqrt{B(E\lambda; I_i \to I_f)} \ , \tag{S22}$$

where $A(t)$ is the time-dependent amplitude of the vector potential and k denotes the photon wave number.

Assuming a linearly polarized laser pulse with wavelength 800 nm, peak intensity 10^{16} W/cm^2, and a Gaussian temporal envelope of 30 fs (FWHM in intensity), the calculated photoexcitation probability is shown in Fig. S3 (a). The excitation probability is found to be on the order of 10^{-45} for a single nucleus during the laser pulse. Due to the substantial detuning between the laser photon energy of 1.55 eV and the isomeric energy of 76.7 eV, the calculated laser excitation probability is so minuscule that the effect of direct laser excitation can be safely neglected.

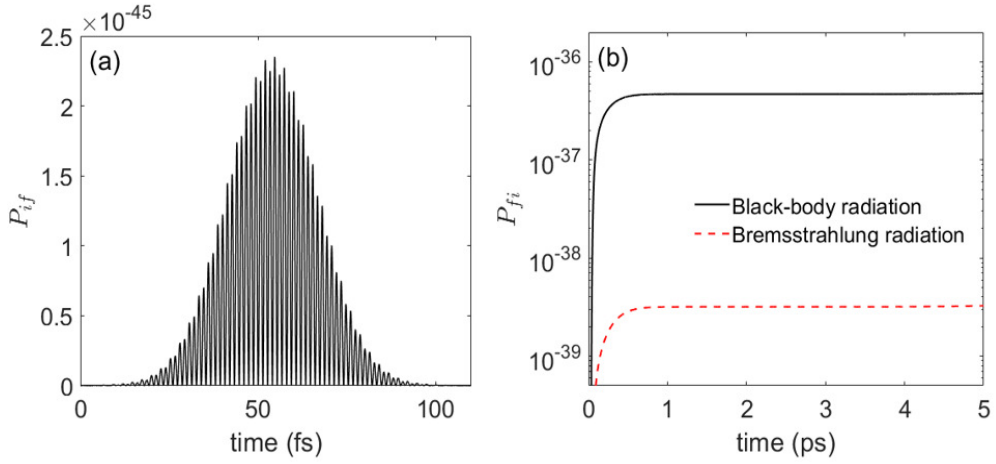

FIG. S3: (a) Photoexcitation probability of a single ^{235}U nucleus induced by the fs laser pulse. The laser has wavelength 800 nm, duration 30 fs, and peak intensity 10^{16} W/cm^2. (b) Photoexcitation probabilities of a single ^{235}U nucleus through blackbody radiations and bremsstrahlung.

3.2 Photoexcitation by blackbody radiations and by bremsstrahlung

In addition to the laser excitation, photoexcitation via blackbody radiations and bremsstrahlung, characterized by broad spectra, is also taken into account. Nuclei within the cluster can undergo excitation through the absorption of photons resonant with the isomeric state. The photoexcitation cross section is computed using the formula [S12]:

$$\sigma_\gamma^{i\to f}(\varepsilon) = \frac{\pi}{2}\frac{2I_f+1}{2I_i+1}\Lambda^2\frac{\Gamma_\gamma\Gamma_t}{(\varepsilon-\varepsilon_{\rm is})^2+\Gamma_t^2/4}\ , \tag{S23}$$

where I_i and I_f are the nuclear spins of the nuclear ground state and nuclear isomeric state, respectively. $\Lambda = h/\varepsilon_{\rm is}$ is the transition wavelength, Γ_γ is the gamma decay width of the nuclear isomeric state, Γ_t is the total decay width, ε is the photon energy, and $\varepsilon_{\rm is}$ is the isomeric energy. Then the photoexcitation probability is calculated with:

$$\begin{aligned} W_\gamma &= \int \sigma_\gamma^{i\to f}(\varepsilon)\phi_\gamma(\varepsilon,T_e)d\varepsilon\ , \\ &= \frac{2I_f+1}{2I_i+1}(\pi\Lambda)^2\Gamma_\gamma\phi_\gamma(\varepsilon_{is},T_e)\ , \end{aligned} \tag{S24}$$

where ϕ_γ is the photon flux. In the laser-cluster interaction scheme, the temperature is a time-dependent function and decreases as the cluster expands. Therefore, the photoexcitation probability for a single ^{235}U nucleus is calculated using $P_{if}(t) = \int_0^t W_\gamma(t')dt'$.

For the case of blackbody radiations, the temperature-dependent photon flux is given by the

expression:

$$\phi_{\gamma}^{\text{blackbody}}(\varepsilon, T_e) = cN_{\gamma}^{\text{Planck}}(\varepsilon, T_e) = \frac{\varepsilon^2}{\pi^2 c^2 \hbar^3 [e^{\varepsilon/T_e} - 1]} \ . \tag{S25}$$

For the case of bremsstrahlung, the photon flux has the form as a function of electron density n_e and temperature T_e [S13]:

$$\phi_{\gamma}^{\text{bremsstrahlung}}(\varepsilon, T_e, n_e) = \int \frac{d\sigma_{\text{bremsstrahlung}}}{d\varepsilon} \phi_e(E_e, T_e, n_e) dE_e \ , \tag{S26}$$

where $d\sigma_{\text{bremsstrahlung}}/d\varepsilon$ denotes the bremsstrahlung differential cross section, as defined by formula 3CS(a) in Ref. [S14]. The term $\phi_e(E_e, T_e, n_e) = n_e f(E_e) v_e(E_e)$ is the electron flux.

Fig. S3(b) shows $P_{if}(t)$ induced by blackbody radiations and bremsstrahlung, ranging between 10^{-39} and 10^{-37}, after exposure to a laser pulse with a peak intensity of 10^{16} W/cm^2. The results indicate that the photoexcitation of nuclei is negligible compared to NEEC.

4. Recombination during nuclear excitation

Recombination processes happen in the laser-generated nanoplasma influencing the ionization equilibrium and thermal balance. Two dominant recombination processes are considered in this study, one is radiative recombination (RR) and the other is three-body recombination (TBR).

4.1 Radiative recombination

RR is one of the primary recombination processes, which occurs when an electron recombines with an ion and emits a photon. The earliest and most prominent RR cross section formula was given by Kramers [S15]. In the current study, we adopt an improved formula of RR rate coefficient from Ref. [S16]:

$$\alpha_{nl}^{\text{RR}}(Z_{\text{eff}}, \Theta) \simeq \left(\frac{3.43 \times 10^{-15}}{n} + \frac{6.03 \times 10^{-14}}{n^2} \right) \frac{Z_{\text{eff}}}{\sqrt{\Theta}} \exp\left[-\frac{(l - 0.711 - 0.372n)^2}{0.308 + 0.431n + 0.0477n^2} \right] \quad (\text{cm}^3 \cdot \text{s}^{-1}) \tag{S27}$$

where n and l are the principal and the angular momentum quantum number of the recombined ion state, respectively. $\Theta = T_e/Z_i^2$ Ryd is a parameter related to electron temperature T_e and effective charge Z_{eff}. A simple form of effective charge is $Z_{\text{eff}} \simeq (Z_C + Z_i)/2$ for $Z_i > Z_C/2$ and $Z_{\text{eff}} \simeq \sqrt{Z_C Z_i}$ for $Z_i < Z_C/2$, where Z_C and Z_i are the nuclear core charge and charge of the ion, respectively.

For an ion with charge Z_i, the RR rate for an electron from free state to a bound state with quantum number n and l is

$$\Gamma_{nl}^{\mathrm{RR}}(n_e, Z_{\mathrm{eff}}, \Theta) = n_e \alpha_{nl}^{\mathrm{RR}}(Z_{\mathrm{eff}}, \Theta) \quad (\mathrm{s}^{-1}), \tag{S28}$$

where n_e is the electron density in cm^{-3}.

4.2 Three-body recombination

TBR is another important recombination process in plasma dynamics, where two free electrons interact within the ionic field. In this interaction, as one of the continuum electrons loses its kinetic energy and is captured, the excess energy released is conveyed to another electron. Hahn derived an empirical formula for the TBR rate, which is adopted as [S17]:

$$\beta^{\mathrm{TBR}}(n_e, Z_i, T_e) \simeq 1.8 \times 10^{-4} T_e^{-1} n_e^{5/6} n_i \Gamma_{\mathrm{G}} Z_i^{-4} \quad (\mathrm{cm}^{-3} \cdot \mathrm{s}^{-1}), \tag{S29}$$

where T_e represents the electron temperature in Rydberg units, and n_i denotes the ion density in cm^{-3}. Here Γ_{G} is called a Gaunt factor, set to be 2. For an electroneutral plasma, $n_e = Z_i n_i$ is satisfied. Eq. (S29) can be witten as

$$\beta^{\mathrm{TBR}}(n_e, Z_i, T_e) \simeq 1.8 \times 10^{-4} T_e^{-1} n_e^{11/6} \Gamma_{\mathrm{G}} Z_i^{-5} \quad (\mathrm{cm}^{-3} \cdot \mathrm{s}^{-1}). \tag{S30}$$

The TBR rate for an ion with charge Z_i is

$$\Gamma^{\mathrm{TBR}}(n_e, Z_i, T_e) = n_e^{-1} \beta^{\mathrm{TBR}}(n_e, Z_i, T_e), \tag{S31}$$

$$\simeq 1.8 \times 10^{-4} T_e^{-1} n_e^{5/6} \Gamma_{\mathrm{G}} Z_i^{-5} \quad (\mathrm{s}^{-1}). \tag{S32}$$

TBR often emerges as the dominant mechanism leading to the capture into high Rydberg states. In high-density plasma, the effects of density-dependent cutoff for high Rydberg states have been taken into consideration.

4.3 Effects of recombination on ion charge states

Recombination processes are not inherently included in Particle-In-Cell (PIC) simulations. In this study, we assess the impact of recombination on ion charge states by calculating recombination rates using the formulas provided in Eq. (S28) and Eq. (S31), along with the density, temperature, and ion charge data derived from the PIC simulation. These time-dependent RR and TBR rates,

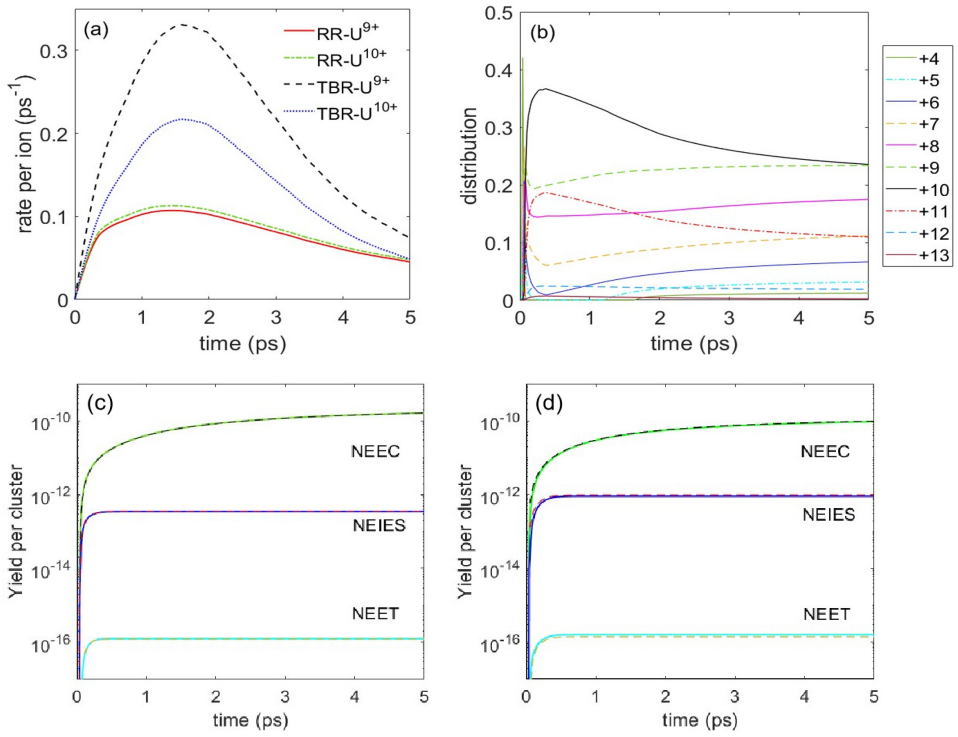

FIG. S4: (a) Time-dependent recombination rates per ion for U^{9+} and U^{10+}, corresponding to the temperatures shown in Fig. 1(c) of the manuscript. The laser parameters are: wavelength 800 nm, duration 30 fs, and peak intensity 5×10^{15} W/cm^2. (b) Updated time-dependent ion charge states of ^{235}U ions in the laser-generated cluster plasma. Isomer production yields via NEEC, NEIES, and NEET are presented with (dashed lines) and without (solid lines) accounting for the effects of recombination: (c) with laser wavelength 800 nm, duration 30 fs, and peak intensity 5×10^{15} W/cm^2; (d) with laser wavelength 800 nm, duration 30 fs, and peak intensity 1×10^{16} W/cm^2.

used to correct ion charge states, enable the determination of updated ion charge states that account for the effects of recombination.

To illustrate the calculation of recombination effects on ion charge states, consider a laser pulse with an intensity of 5×10^{15} W/cm^2 and a duration of 30 fs. The typical electron temperature within the ^{235}U cluster, as determined by the PIC simulation, is approximately 10 eV, as shown in Fig. 1(c) of the manuscript. For the predominant ions, U^{9+} and U^{10+}, the time-dependent RR and TBR rates are presented in Fig. S4(a), while the updated time-dependent ion charge states for U^{9+} and U^{10+} are illustrated in Fig. S4(b).

The updated time-dependent ion charge states, which account for the effects of recombination, are now used to calculate isomer production. Figures S4(c) and (d) compare the isomer production as a function of cluster expansion time, with and without considering recombination effects, and

they show only minor differences in most cases. This is because nuclear excitation mainly occurs within the first few hundred fs, during which ionization effects dominate over recombination.

---

* J. Q. and B. L. contributed equally to this work.

† xwang@gscaep.ac.cn

[S1] K. Alder, A. Bohr, T. Huus, B. Mottelson, and A. Winther, Study of nuclear structure by electromagnetic excitation with accelerated ions, Rev. Mod. Phys. **28**, 432 (1956).

[S2] J. M. Blatt and V. F. Weisskopf, *Theoretical nuclear physics* (Verlag, New York, 1979).

[S3] J. C. Berengut, Resonant Electronic-Bridge Excitation of the ^{235}U Nuclear Transition in Ions with Chaotic Spectra, Phys. Rev. Lett. **121**, 253002 (2018).

[S4] M. Rose, *Relativistic Electron Theory* (Wiley, New York, 1961).

[S5] H. Zhang, W. Wang, and X. Wang, Nuclear excitation cross section of ^{229}Th via inelastic electron scattering, Phys. Rev. C **106**, 044604 (2022).

[S6] B. Liu and X. Wang, Isomeric excitation of ^{235}U by inelastic scattering of low-energy electrons, Phys. Rev. C **106**, 064604 (2022).

[S7] H. Zhang and X. Wang, Theory of isomeric excitation of ^{229}Th via electronic processes, Front. Phys. **11**, 1166566 (2023).

[S8] H. R. Griem, *Plasma Spectroscopy* (McGraw-Hill, New York, 1994).

[S9] P. J. Chantry, Doppler broadening in beam experiments, J. Chem. Phys. **55**, 2746 (1971).

[S10] F. Salvat and J. M. Fernandez-Varea, radial: A Fortran subroutine package for the solution of the radial Schrdinger and Dirac wave equations, Comput. Phys. Commun. **240**, 165 (2019).

[S11] A. Pálffy, J. Evers, and C. H. Keitel, Electric-dipole-forbidden nuclear transitions driven by superintense laser fields, Phys. Rev. C **77**, 044602 (2008).

[S12] M. R. Harston and J. F. Chemin, Mechanisms of nuclear excitation in plasmas, Phys. Rev. C **59**, 2462 (1999).

[S13] J. Gunst, Y. Wu, C. H. Keitel, and A. Pálffy, Nuclear excitation by electron capture in optical-laser-generated plasmas, Phys. Rev. E **97**, 063205 (2018).

[S14] H. W. Koch and J. Motz, Bremsstrahlung cross-section formulas and related data, Rev. Mod. Phys. **31**, 920 (1959).

[S15] H. A. Kramers, On the theory of X-ray absorption and of the continuous X-ray spectrum, Philos. Mag. **46**, 836 (1923).

[S16] Y. Hahn, Electron-ion recombination processes-an overview, Rep. Prog. Phys. **60**, 691 (1997).

[S17] Y. Hahn, Plasma density effects on the three-body recombination rate coefficients, Phys. Lett. A **231**, 82 (1997).